Title

A Safer, Wide-Temperature Liquefied Gas Electrolyte Based on Difluoromethane

Authors

Davies, Daniel M
Yang, Yangyuchen
Sablina, Ekaterina S
et al.

Publication Date

2021-05-01

DOI

10.1016/j.jpowsour.2021.229668

Peer reviewed

A Safer, Wide-Temperature Liquefied Gas Electrolyte Based on Difluoromethane

Daniel M. Davies [a], Yangyuchen Yang [b], Ekaterina S. Sablina [a], Yijie Yin [b], Matthew Mayer [b], Yihui Zhang [a], Marco Olguin [a], Jungwoo Z. Lee [e], Bingyu Lu [a], Dijo Damien [f], Oleg Borodin [c,d,***], Cyrus S. Rustomji [e,**], Y. Shirley Meng [a,b,g,*]

[a] *Department of Nano Engineering, University of California San Diego, La Jolla, CA, 92121, USA*
[b] *Materials Science and Engineering, University of California San Diego, La Jolla, CA, 92121, USA*
[c] *Electrochemistry Branch, Sensors and Electron Devices Directorate, U.S. Army Research Laboratory, Adelphi, MD, 20783, USA*
[d] *Joint Center for Energy Storage Research, U.S. Army Research Laboratory, Adelphi, MD, 20783, USA*
[e] *South 8 Technologies, Inc., San Diego, CA, 92109, USA*
[f] *Christ College Irinjalakuda, Kerala, 680125, INDIA*
[g] *Sustainable Power and Energy Center (SPEC), University of California San Diego, La Jolla, USA*

HIGHLIGHTS

- Demonstration of unique safety feature inherent to liquefied gas electrolytes.
- Low flammability, difluoromethane based solvent enables wide temperature operation.
- Raman spectroscopy reveals few free co-solvent molecules and high salt aggregation.
- MD simulations compliment experimental results with insight into Li^+ transportation.
- Li.|Cu plating/stripping and full cells operational through a wide temperature range

ARTICLE INFO

Keywords:
Safety
Liquefied Gas Electrolyte
Solvation Structure
Lithium Metal

ABSTRACT

Development of safe electrolytes that are compatible with both lithium metal anodes and high-voltage cathodes that can operate in a wide-temperature range is a formidable, yet important challenge. Recently, a new class of electrolytes based on liquefied gas solvents has shown promise in addressing this issue. Concerns, however, have been raised on the pressure, flammability and low maximum operating temperature of these systems. Here, we endeavor to mitigate safety and practicality concerns by demonstrating an enhanced safety feature inherent in liquefied gas electrolytes and by showing the viability of using difluoromethane as a liquefied gas solvent which has lower pressure, lower flammability, and improved maximum operation temperature characteristics compared with fluoromethane. We create a custom-built setup to enable liquefied gas electrolyte characterization through Raman spectroscopy and supplement this with molecular dynamics (MD) simulations. The electrolyte shows good conductivity through a wide temperature range and compatibility with both the lithium metal anode and 4 V class cathodes. The demonstrated use of such alternative liquefied gas solvents opens a path towards the further development of high-energy and safe batteries that can operate in a wide-temperature range.

1. Introduction

Batteries are ubiquitous today in a vast number of applications. They vary greatly in size and application, from portable electronics to providing energy storage for grid reliability and resiliency. The front running chemistry for a number of these applications is the

* Corresponding author. Department of Nano Engineering, University of California San Diego, La Jolla, CA, 92121, USA.
** Corresponding author.
*** Corresponding author. Electrochemistry Branch, Sensors and Electron Devices Directorate, U.S. Army Research Laboratory, Adelphi, MD, 20783, USA.
E-mail addresses: oleg.a.borodin.civ@mail.mil (O. Borodin), crustomji@south8technologies.com (C.S. Rustomji), shmeng@ucsd.edu (Y.S. Meng).

intercalation-based lithium-ion battery, which has received a great deal of attention in the last few decades [1–3]. Scientists are nearing the theoretical limits of conventional (graphite-based anode) intercalation chemistries [4]; however, there is still a demand for next-generation batteries with higher energy density to meet expanding needs. Using lithium metal (Li-metal) as the anode has been touted as the next great step in producing batteries with higher energy densities [5]. This is primarily due to Li-metal's much higher theoretical capacity density than that of graphite. Further, it provides a lithium source, which opens the possibility of using cathodes that do not provide their own lithium, including promising cathode systems such as sulfur or oxygen [6]; however, adoption of rechargeable Li-metal batteries has been limited due to low Coulombic efficiencies (CEs), dendrite growth, large volume change during cycling [7], and safety concerns.

Recently, electrolyte development has received a lot of attention as a possible pathway to achieving stable Li-metal interfaces and cell performances. However, researchers also need to consider the safety and the operation temperature and power of the electrolytes in order to expand the boundaries of practical, high-energy density batteries. Although conventional carbonate-based electrolytes have high oxidation stability (4.3 V vs. Li) [8]' they display poor compatibility with Li-metal anodes and are known to be highly flammable [9]. Ether-based electrolytes cycle with relatively high CEs; however, their use is limited by low oxidation stability (<4.0 V vs. Li) [10]. Low molecular weight ethers are also highly flammable.

More recently, high-concentration electrolytes have been shown to form LiF-rich SEIs through salt decomposition and high CE cycling of Li-metal has been demonstrated with these electrolytes. Further advances in this field have brought about locally highly-concentrated electrolytes which partially mitigate some of the disadvantages of highly-concentrated electrolytes – namely their cost, viscosity, wettability, and poor performance at low temperatures [11]. In addition, in recent years there has been a large amount of interest in solid-state electrolytes (SSEs) for Li-metal based batteries; however, these electrolytes also have been hindered by low conductivity at low (and even ambient) temperatures [12].

Along with the focus on both liquid and solid electrolytes, lately there have been developments with solvents that are gaseous at ambient temperature and pressure [13–15]. At moderate pressures or low temperatures these gaseous molecules can be liquefied, functioning as solvents that can dissolve Li salts to form liquefied gas electrolytes (LGEs). In these articles, successful cycling of Li-metal using fluoromethane (CH_3F, FM)–based electrolytes with dendrite-free morphology and high CE has been presented. The low melting point, low viscosity, inherent pressure, electrochemical stability, and high donatable fluorine content [16] combine synergistically to enable excellent Li-metal performance, even down to temperatures as low as − 60 °C. However, there has been uneasiness about the practicality and safety of LGEs. Along with worries about the manufacturability of batteries utilizing LGEs, the three factors of most concern are the inherently high internal pressure, flammability, and low critical point of the solvent.

Here, we demonstrate results and progress towards alleviating concerns regarding the practicality and safety of using LGEs. First, we present an enhanced safety feature inherent in LGEs by showing the results of a nail-penetration test on a full Li-ion cell in an 18650 form-factor cycled with an LGE. Next, we demonstrate the potential of using LGEs with difluoromethane (CH_2F_2, DFM) as the primary solvent, which exhibits improved safety features and operational temperature range. We use computational and spectroscopic techniques to help understand the solvation and transport of these electrolytes. The electrolytes shows impressive conductivity between − 60 and + 70 °C and compatibility with both the Li Metal anode and 4 V class Lithium Nickel Cobalt Manganese Oxide ($LiNiCoMnO_2$, NMC)cathodes. By demonstrating this enhanced safety feature and the viability of using a low-flammability solvent, we lower the barriers of adoption for developing safe and practical LGEs.

1.1. Inherent safety feature of liquefied gas electrolytes

The nail penetration test has been widely used by battery companies, automotive manufacturers, and other battery users [17]. This test involves driving a nail through the battery, consequently creating a short circuit. In conventional Li-ion batteries, the short circuit in this test typically results in heating of the battery, often leading to thermal runaway, with the battery generally displaying smoke, fire, or even exploding shortly after the nail penetration [18]. Such tests are typically conducted on batteries in conventional, practical form factors such as pouch or cylindrical cells. It has been shown that the likelihood of a battery undergoing a thermal event is substantially increased when the nail penetration location is central and the battery is at a high state of charge [19].

To test the effects that the different physio-chemical properties of LGEs would have on the nail penetration test, we used a battery containing conventional electrode materials (Graphite Anode, NMC cathode in a cylindrical 18650 format. Using a custom designed cap [20] and electrolyte insertion process we filled the cell with an LGE - 0.3 M Lithium bis(trifluoromethanesulfonyl)imide (LiTFSI), 0.3 M tetrahydrofuran (THF), in 19:1 FM:CO_2. The 18650 cell underwent three full cycles and was fully charged to 4.2 V, before nail penetration was performed in the center (horizontal axis) of the jelly roll.

The results of the nail penetration test are displayed in Fig. 1. The approximate time of penetration during the test is indicated by the sharp decrease in cell voltage to 0 V. During nail penetration with the LGE, two important observations were made. First, immediately after penetration the non-toxic solvent rapidly evaporated and escaped. This is supported by the temperature profile seen in the nail penetration results. In conventional Li-ion batteries with liquid electrolytes, after nail penetration, the temperature of the cell often rises rapidly. In contrast, in our system containing an LGE, during the penetration we saw a sharp decrease in the temperature of the cell to below −10 °C due to the cooling effect of the swiftly expanding gas escaping from the cell. The cell temperature then stabilized back to approximately room temperature and no sparks or flames were observed throughout the test. The second, less obvious effect, was that the ionic conductive pathway was eliminated as a result of the gas dissipating. Once the bulk solvent had been removed, there no longer was a medium in which the Li-ions could transport between the electrodes, and consequently short-circuiting of the battery was prevented. This behavior is characteristic of LGEs due to their inherently high volatility and results in a distinctive safety feature unique to this class of electrolytes. Regardless of whether the primary solvent is FM or another liquefied gas, the effect is expected for solvents with sufficiently high volatility. Similarly, under other physical abuse such as overcharge or high temperature exposure, the cell may avoid thermal runaway by safely venting.

1.2. Liquefied gas electrolyte based on difluoromethane

The low-melting point, low viscosity, high-voltage stability and high presence of fluorine are properties of FM that have combined synergistically to give impressive performance of electrolytes based on this solvent [14,15,21]. DFM maintains many of the beneficial properties of FM, including the low-melting point, low-viscosity, and relatively high dielectric constant (Table S1) and other physical-chemical properties shown in Fig. 2a. Notably, at +20 °C, the vapor pressure of DFM (14.6 atm) is less than half that of FM (33.6 atm). Additionally, the critical temperature of DFM (+78.5 °C) is significantly higher than that of FM (+44.5 °C) [22]. As is shown previously [13,14], this value is important for the high temperature conductivity of LGEs, especially with low salt concentrations. The table also shows interesting properties regarding the flammability of the two substances which are detailed below.

The American Society of Heating, Refrigerating and Air-Conditioning Engineers (ASHRAE) standard 34 (ISO 817:2014) classifies the flammability of a refrigerant in 4 different categories: 1 (non-

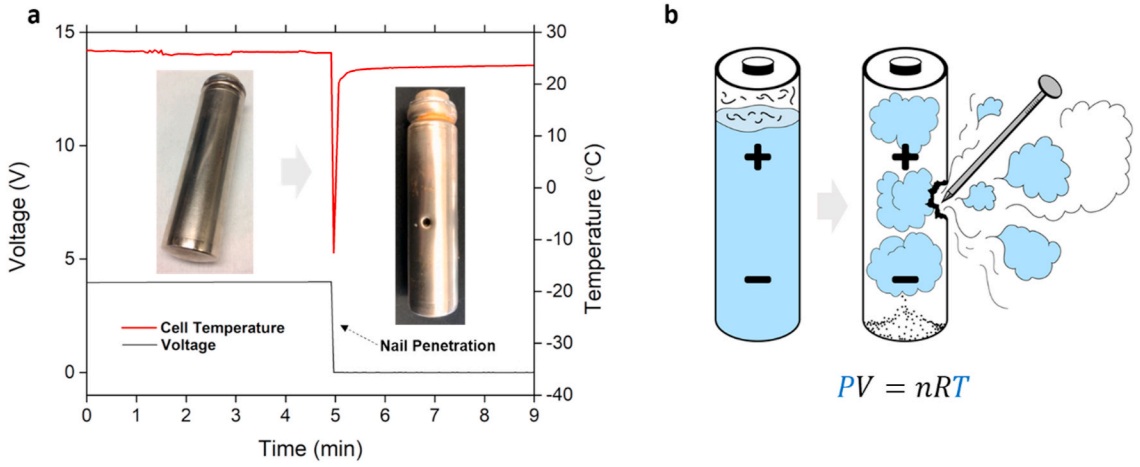

Fig. 1. Nail Penetration of an 18650 Form-Factor Cell with Liquefied Gas Electrolyte. (a) The voltage (black) and cell temperature (red) during a nail penetration test of a Graphite-NMC Li-ion battery in an 18650 form-factor filled with an LGE. The inset images show an 18650 cell before (left) and after (right) nail penetration. (b) schematic of the liquefied gas evaporating and expanding after nail penetration. The cell cooling is a direct result of the Ideal Gas Law. Salt remains in the cell after solvent evaporation. (For interpretation of the references to colour in this figure legend, the reader is referred to the Web version of this article.)

a

Property	Flurometh ane	Difluoromethane
Chemical Structure		
Vapor Pressure @ 20°C (atm)	33.6	14.6
Critical Temperature (°C)	44.5	78.5
Lower Flammability Limit (v/v %)	5.6	14.4
Upper Flammability Limit (v/v %)	22.2	33
Maximum Burn Velocity ($cm \cdot s^{-1}$)	28.2	6.7
Heat of Combustion ($MJ \cdot kg^{-1}$)	19.8	9.4
GWP 100	116	677

b

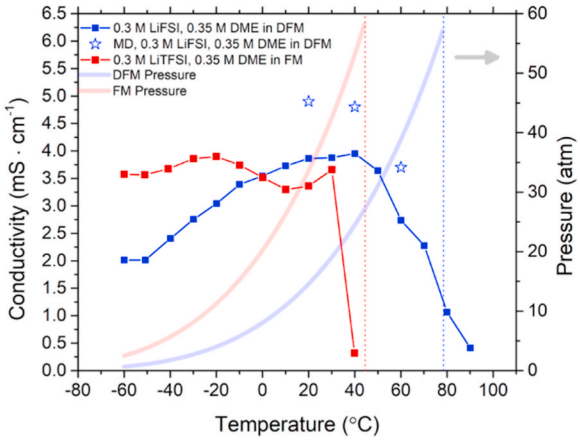

Fig. 2. Physical-chemical properties of fluoromethane and difluoromethane (a) comparison of the physical-chemical properties of Fluoromethane and Difluoromethane. In the chemical structure the hydrogen is white, carbon is grey, and fluorine is green. GWP100 is an indication of how much energy is absorbed by the greenhouse gas over 100 years relative to CO_2 [24–27,29–31,34] (b) The conductivity of 0.3 M LiTFSI, 0.35 M DME in FM (red scatter & line) and 0.3 M LFSI, 0.35 M DME in DFM (blue scatter & line). The blue stars show the predicted conductivity from MD simulations of the DFM-based electrolyte (0.3 M LFSI, 0.35 M DME in DFM), replica 2 from Table S3. The partially transparent lines show how the vapor pressure of the solvents – FM (red), DFM (blue) vary with temperature. The dotted lines show the critical temperatures of the solvents – FM (red), DFM (blue). (For interpretation of the references to colour in this figure legend, the reader is referred to the Web version of this article.)

flammable), 2L (low flammability), 2 (flammable), and 3 (high flammability) [23,24] with the prefix "A" indicating that the solvent is non-toxic. Likely due to a small worldwide usage in refrigeration applications, FM does not have an official ASHRAE classification. Given its heat of combustion (19.8 MJ kg^{-1}) [25], lower flammability limit 5.6 (v/v %) [26], and laminar burn velocity (28.2 cm/s) [25], it is predicted that it would be classified into group A3[27].

On the other hand, DFM is widely used as a refrigerant [28] and has been assigned the designation A2L – reserved for low toxicity refrigerants that are difficult to ignite or sustain a flame [23]. The class 2L is distinguished from 2 by the requirement that the laminar burning velocity of the refrigerant must be below 10 cm/s. With its low laminar burn rate (6.2 cm/s) [29], low heat of combustion (9.4 MJ kg^{-1}) [30], and its relatively high flammability limit (14.4%) [31] DFM is increasingly being used as a refrigerant worldwide – both in blends, and is being explored as stand-alone option [32]. It is important to note here that conventional electrolytes such as $LiPF_6$ salt in mixtures of ethylene carbonate and dimethyl carbonate solvents are highly flammable and pose other significant safety risks [33]. The possibility of using low flammability solvents, combined with the inherent safety features of LGEs provide an unexpected pathway towards high performing, safe electrolytes.

Due to these advantageous properties of DFM, the reader may question why previous efforts with LGEs have focused on FM rather than DFM. This is because the solubilities of Li salts are generally lower in DFM than FM [13]. Recently, use of co-solvents (at ratios near 1:1 – co-solvent:salt), have been used to further improve the solubility of FM-based LGEs [14,15]. A similar approach is expected to improve the solubility of Li salts in DFM. A systematic study (summarized in Table S2) was conducted using a variety of salts, co-solvents and concentrations to try to identify the most promising LGE candidates. We found that at 1:1 ratios of co-solvent to salt, both LiTFSI and Lithium bis (fluorosulfonyl)imide (LiFSI) were unable to fully dissolve in DFM. By slightly increasing the ratio of co-solvent to salt, we were able to fully dissolve both LiTFSI and LiFSI salts. It is important to note that although in some cases there is twice as much co-solvent as salt on a molar basis,

these systems would still qualify as "locally highly concentrated" electrolytes [35]. By using a low ratio of co-solvent:salt we ensure that the co-solvents are complexed to Li^+ cations and there are limited "free" co-solvents resulting in higher electrolyte resistance to oxidation [36]. After creating and performing preliminary electrochemical testing on a number of electrolytes (Fig. S1) we decided to explore in detail systems using 1,2 dimethoxymethane (DME) as the co-solvent, and LiFSI as the salt. These systems were studied as the co-solvent:salt ratio required to dissolve the salt was small and the systems yielded promising electrochemical performance, which is further detailed in a later section (Fig. 4).

Fig. 2b shows a comparison of the conductivities of electrolytes based on FM and DFM through wide temperature ranges, as well as the corresponding vapor pressures of the primary solvents in the respective temperature range. For the FM-based electrolyte, we see high conductivity (>3 mS m^{-1}) from − 60 to +30 °C, followed by a drop in conductivity at +40 °C (near the critical point of the electrolyte) consistent with previous results [14,21]. The DFM based electrolyte has a similarly high conductivity at low temperatures (>2 mS cm^{-1}) at − 60 °C, with a reduction in conductivity seen at the much higher temperature of approximately +70 °C. This increased conductivity for the DFM-based electrolyte compared to the FM-based ones at high temperatures is attributed to the higher critical temperature of DFM than FM. As the electrolyte approaches the critical temperature, the amount of solvent in the liquid phase significantly reduces due to the increased density of the vapor phase. In the experimental conductivity setup used, it is believed that as this liquid volume is reduced, contact with the electrodes is not maintained, demonstrating a significant drop in conductivity.

1.3. Solvation and transport properties

Due to the pressurized nature of the LGE, it has previously been difficult to physically characterize the electrolytes. For this work, we developed a custom setup that allowed us to perform Raman analysis on the pressurized electrolyte systems. The apparatuses are shown in Fig. S2. To study the solvation structure, we added varying concentrations (0 M–1 M) of LiFSI to 1.3 M of DME in DFM. Usage of higher salt and DME concentrations up to 1.3 M (as opposed to 0.35 M) improved the signal to noise of both the DME and FSI^- peaks in the spectroscopic measurements due to a larger amount of co-solvent and salt.

Fig. 3a shows the peak characteristic of the C–O stretching vibration in the DME molecule. With 0 M of FSI^- (black line), this peak matches with the C–O stretching vibration seen in pure DME [37]. As more FSI^- is introduced, reduction in the normalized intensity of the free DME peak at 850 cm^{-1} occurs and a new peak arises at 874 cm^{-1}, which has previously been correlated with an increase in the coordination of DME to Li^+ [38]. At LiFSI salt concentrations above 0.5 M, the C–O vibrational peak associated with free DME is no longer visible, indicating a strong degree of coordination between the DME and the Li^+. Fig. 3b shows the characteristic peak of FSI^-. At low concentrations the peak is centered approximately around 725 cm^{-1}, which is consistent with previous literature [39]. With an increase in FSI^- concentration we see a shift in the characteristic peak to be centered around 750 cm^{-1}. This shift in the FSI^- peak has previously been attributed to an increase in aggregation of FSI^-, indicating a large amount salt aggregation in the electrolyte [40,41]. In previous LGEs this high aggregation has led to very few free $TFSI^-$ anions (<0.1%) [14,15], however, in this system we still see a significant portion of free anions (Fig. S3a). Higher mobility of free FSI^- compared to free Li^+ and ions participating in ion pairing and aggregates (Fig. S3b) leads to significant contribution anions to charge transport and to a lower transference number (Fig. S4) than reported in the FM based electrolytes. Finally, Fig. 3c shows the C–F stretching peak of DFM. We see that with increasing LiFSI concentration there is no shift of the peak from 527 cm^{-1}, but peak broadening is apparent. This indicates that very little DFM is coordinated with the Li ions in their first coordination shell, which is in contrast to the significant participation of

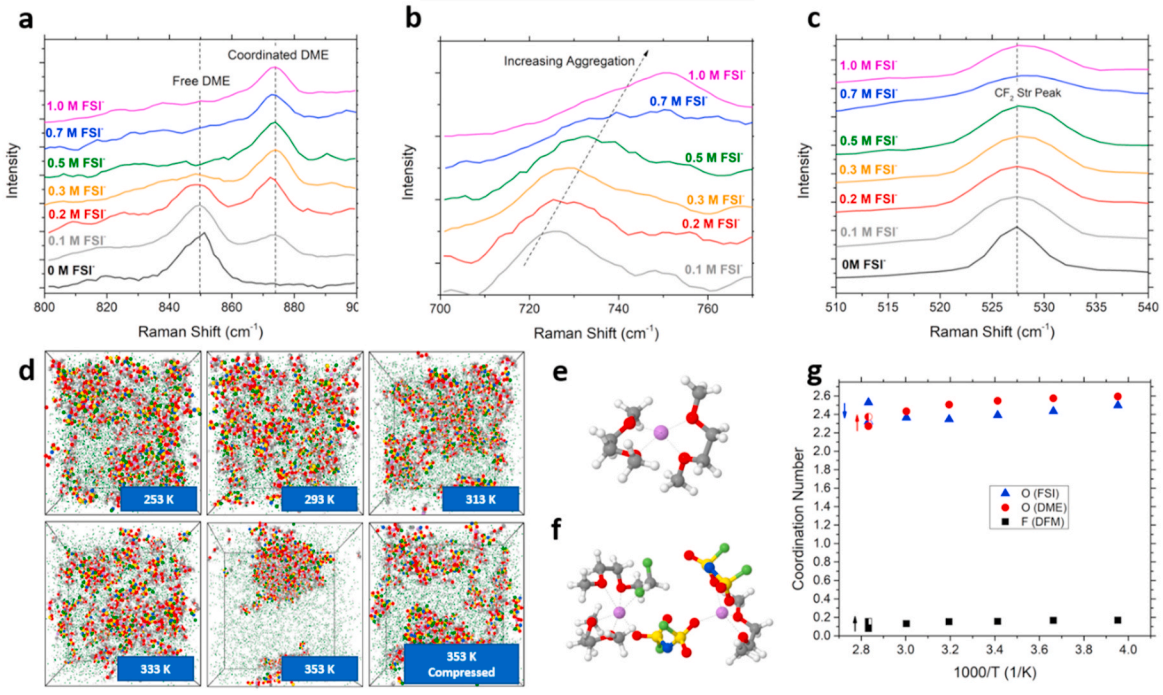

Fig. 3. Spectroscopic and Characterization of the DFM-based electrolyte. (a–c) Raman spectra of LGEs with 1.3 M DME and increasing LiFSI concentrations in 800–900 cm^{-1} (DME C–O stretching peak), 700-790 cm^{-1} (LiFSI characteristic peak), and 510-540 cm^{-1} (DFM C–F stretching peak). (d) Snapshots of electrolyte systems at various temperatures. Size of DFM molecules lowered. (e, f) representative solvation structures of Li^+ from the simulations. (d) shows Li^+ surrounded by 2 DME molecules. (e) shows 2 Li^+ surrounded by 3 DME, 1 DFM, and 2 LiFSI molecules. (g) Coordination number of Li^+ at various temperatures. Lithium: purple, oxygen: red, carbon: grey, hydrogen: white, fluorine: green, nitrogen: blue, sulfur: yellow. (For interpretation of the references to colour in this figure legend, the reader is referred to the Web version of this article.)

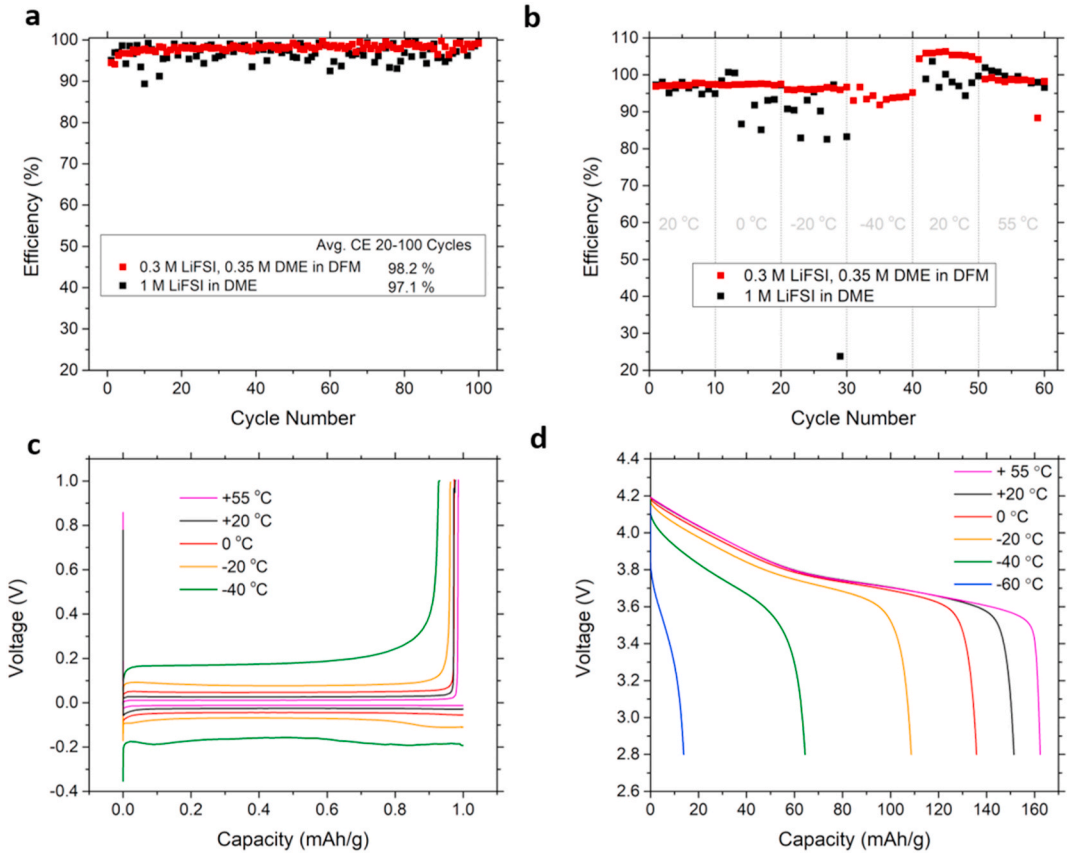

Fig. 4. Electrochemical performance of the Li metal anode in the liquefied gas electrolyte in a wide temperature range LGE used: 0.3 M LiFSI,0.35 M DME in DFM (a) The CE of Li metal plating/stripping over 100 cycles at 0.5 mA/cm^2,1.0 mA h/cm [2]. LGE: red; 1 M LiFSI in DME: black. (b) The CE of Li metal plating/stripping (at 0.5 mA/cm^2,1.0 mA h/cm^2) at various temperatures. LGE: red; 1 M LiFSI in DME: black (c) voltage profiles for the LGE cell in (b). (d) Li-NMC 622 cell cycled at a rate of C/20 at temperatures of +20 °C, 0 °C, −20 °C, −40 °C, −60 °C, and then +55 °C with the LGE. (For interpretation of the references to colour in this figure legend, the reader is referred to the Web version of this article.)

FM in the first solvation shell of FM based systems [15]. These results indicate that the Li^+ is largely coordinated by DME, and FSI^-, forming substantial aggregates, with DFM participating infrequently in the first solvation shell.

Molecular dynamics (MD) simulations were performed on the DFM-based electrolytes for two salt/co-solvent concentrations: 1 M LiFSI, 1.3 M DME in DFM and 0.3 M LiFSI, 0.35 M DME in DFM. We observed similar ion solvation trends and transport mechanisms for both salt concentrations and, therefore, focus our discussion only on the higher salt concentration for simplicity. Analysis of the Li^+ coordination via the radial distribution functions (RDFs) (see Fig. S5) revealed a strong preference for Li^+ coordination by the oxygen of DME, followed by the oxygen of the FSI^- and only week coordination with DFM fluorine atoms. Fig. 3g shows a composition of the Li^+ first solvation shell (at 2.8 Å) at different temperatures. At room temperature, a Li^+ cation, on average, is coordinated to 2.5 O (DME) out of 2.6 available due to DME: Li = 1.3 ratio, 2.4 O (FSI^-), and 0.16 F (DFM). This indicates that almost all the DME is coordinated to Li^+ and that DFM has little participation in the first solvation shell of Li^+, consistent with the Raman results shown in Fig. 3a and c. Fig. 3e shows a representative solvate for a free Li^+, while Fig. 3f shows a representation of an ionic aggregate. Representative snap shots of the simulation cell at different temperatures are shown in Fig. 3d. In agreement with to the FM based electrolytes, we see an increase in aggregation with temperature [14,15]. This aggregation and disappearance of the solvent separated free ions contributes to the eventual conductivity loss of the electrolyte at high temperatures that is accurately predicted by MD simulations (see Fig. S6 and Fig. 2b). Specifically, the degree of ion correlation (a_d) that is often called ionicity decreases with increasing temperature (Fig. S7). This decrease partially compensates for the increase in diffusion coefficients of the molecules at lower temperatures (Fig. S8) leading to the relatively flat conductivity curve through a wide temperature range. Note that in addition to MD simulations at the experimental densities, we performed MD simulations of a compressed electrolyte at +80 °C, having a density approximated from experiments at +60 °C. Electrolyte compression leads to an increase in ionization, free Li^+ cations and conductivity of the electrolyte. It is believed that the actual compression of the electrolyte is somewhere between the two methods used. Future work will focus on more accurate modelling of the electrolyte compression at temperatures near the critical point of liquefied gas solvent but will require even larger simulations cells with a larger number of ions to accurately capture large ion cluster formation.

1.4. Li-metal anode and Li-Metal battery performance

We explored the compatibility of the DFM-based electrolyte by conducting Li-metal plating/stripping tests on Cu electrodes. The SEI formed by DFM with Li, is more stable that the SEI formed by FM (Fig. S9) which eliminates the need to add carbon dioxide in system. 0.3 M LiFSI, 0.35 M DME in DFM (Fig. 4) was used as the DFM-based LGE for electrochemical studies. We also compared the results to a 1 M LiFSI in DME liquid electrolyte.

With the DFM based LGE, we see a first cycle CE of 94.5% which increased to an average CE of 98.2% over 100 cycles (Fig. 4a). The electrolyte demonstrates higher efficiency and better stability cycling of Li-metal than both the 0.3 M LiFSI in DME (93.2%), and the more

common 1 M LiFSI in DME (97.1%). Limited results are also shown for 1 M LiFSI, 1.3 M DME in DFM in Fig. S10. In Fig. 4b we see that stable cycling of Li-metal is possible between − 40 and + 55 °C with this LGE. The performance of the electrolyte at low temperatures is far superior to the conventional ether-based electrolyte, which shows unstable cycling at − 20 °C and was unable to cycle at − 40 °C. After returning to room temperature, we see an average CE of over 100%, likely due to the release of Li + ions previously held by the SEI layer back into the system [14]. Stable, high efficiency cycling is demonstrated at the raised temperature of +55 °C, a temperature previously inaccessible by low-concentration FM-based LGEs. Representative voltage curves during cycling in the LGE are shown in Fig. 4c, which show low, stable over-potentials down to − 20°C with a slight increase in overpotential at −40 °C. Upon returning to +20 °C we see that the voltage curve is almost identical to what it was prior to the low and high temperature cycling. These initial results are promising, and future work will explore methods to further improve the CE through novel electrolyte design such as co-solvents, additives and salts.

To explore the compatibility of the DFM based electrolyte with 4 V class cathodes, we made full Li-metal cells using commercial $LiNi_{0.6}Mn_{0.2}Co_{0.2}O_2$ (NMC622) cathodes with capacity loading of ~1.8 mAh·cm^{-2}. Fig. 4d shows promising wide-temperature, full cell cycling. For these results, the charging temperature was the same as the discharging temperature, therefore including the effects of limited charging kinetics at low temperature. Cycling in the range of −60 to +55 °C is demonstrated with 42% capacity retention at −40 °C (as compared to +20 °C) and good performance shown up to +55 °C. Longer term cycling with 4 V class cathodes is shown in Fig. S11. The capacity degradation seen with the NMC622 cathode in Fig. S11a is thought to be due to the incompatibility of DME with high voltage cathodes. Cycling with a lower voltage cathode $LiFePO_4$ (LFP) yields higher capacity retention (Figs. S11b and S11c). These results show the possibility to design safer LGEs based on alternative solvents to perform in high energy density batteries in wide temperature ranges.

2. Conclusion

In this study we endeavored to quell some of the previous concerns raised about the safety and practicality of using liquefied gas-based electrolytes. First, we demonstrated impressive safety results with 18650 format cells containing LGEs, cooling rapidly under nail penetration. This phenomenon is inherent to the LGEs and is expected to be present in all systems containing these gases (whether the gas is FM, DFM or some other liquefied gas solvent with sufficiently high volatility). Next, we developed an LGE based on DFM as the primary solvent and identified a formulation that helps to mitigate some of the major issues that have arisen with LGEs based on FM. The new DFM-based electrolyte has a lower pressure, lower flammability, and a higher maximum operating temperature than its FM-based predecessors. Importantly, DFM still possesses many of the properties that make FM an attractive solvent, such as low viscosity and a wide electrochemical window. The electrolyte demonstrated good conductivity, as well as Li-metal and 4 V class cathode compatibility through a wide temperature range.

Conventional wisdom suggests that the gaseous nature of LGEs gives rise to significant battery system safety and practicality concerns. In this paper, however, we have shown that the pressurized nature of such LGE systems provides significant and unique safety benefits. By demonstrating the use of, and characterizing an LGE with an alternative, lower pressure, and low-flammability solvent, we also have shown a path forward to explore different LGEs and the potential for these systems to be used in safe and practical high energy density batteries.

3. Experimental

3.1. Materials

The salts Lithium bis(fluorosulfonyl)imide (LiFSI) (99.9%) and lithium bis(trifluoromethane)sulfonimide (LiTFSI) (99.9%) were obtained from BASF. Fluoromethane (99.99%) and Difluoromethane (99.99%) were purchased from commercial sources. 1,2-dimethoxyethane (DME, 99.5%), and 99.8%) were purchased from Sigma-Aldrich and stored over molecular sieves. The NMC622 (A-C023) was obtained from Argonne national laboratory. The LFP was purchased from MTI.

3.2. Electrochemical measurements

Electrolytic conductivity measurements were performed in custom fabricated high-pressure stainless-steel coin cells, using polished stainless-steel (SS 316L) as both electrodes. The cell constant was calibrated from 0.447 to 80 mS cm^{-1} by using OAKTON standard conductivity solutions. Battery cycling tests were performed by an Arbin battery test station (BT2043, Arbin Instruments, USA) in custom designed high-pressure stainless-steel coin cells, with Li metal (FMC Lithium, 1 mm thickness, ¼ inch diameter) as the counter electrode and Cu foil as the working electrode. A single 25 μm porous polypropylene separator (Celgard 2075) was applied for all the electrochemical experiments. For Li metal plating and stripping experiments, lithium was first deposited onto the working electrode at 0.5 mA cm^{-2} until 0 V vs. Li and the voltage was held for 5 h to form a stable SEI on the current collector. The first plating cycle was then started, followed by complete lithium stripping to a 1 V vs. Li cut off voltage. The CE was calculated as the Li stripping capacity divided by the Li plating capacity during a single cycle. For the tests at different temperatures, the cells were stored at the testing temperature in a temperature chamber (Espec) for several hours before cycling. In Li-NMC cycling, the cell was firstly cycled at C/10 rate at room temperature for 2 activation cycles and were subsequently cycled at selected rates and temperatures.

3.3. Electrolyte addition

Electrolyte addition procedures have been described previously [21].

3.4. Material characterization

Raman spectra of liquefied gas electrolytes were carried on Renishaw inVia confocal Raman microscope with an excitation wavelength of 532 nm. All spectra were calibrated with Si (520 nm) and analyzed by Wire 3.4 software developed by Renishaw Ltd.

4. Computational methods

Molecular dynamics simulations were performed using APPLE&P polarizable force fields [42,43]. The LiFSI and DME force field parameters accurately predicted structure and transport properties of the similar DME-LiTFSI and DME-DOL-LiTFSI electrolytes [44]. The Li^+/DFM parameters were developed in this work following previously described methodology by fitting to quantum chemistry data. [45] Charges were fit to electrostatic potential calculated around DFM at the MP2/aug-cc-pvTz level, yielding a DFM dipole moment of 2.12 Debye vs. 2.0 D from MP2/aug-cc-pvTz quantum chemistry calculations. DFM molecular polarizability was 2.5 Å^3 from force field and 2.51 Å^3 from M05-2X/aug-cc-pvTz DFT calculations. Molecular mechanics calculations using developed force field yielded the Li^+/DFM binding energy −25.2 kcal/mol in good agreement with the value of −25.0 kcal/mol from G4MP2 quantum chemistry calculations.

Two systems were simulated. One system was composed of 120

LiFSI, 156 DME, and 1960 DFM molecules corresponding to the 1 M LiFSI, 1.3 M DME in DFM electrolyte. The other system was composed of 32 LiFSI, 38 DME, and 1960 DFM molecules corresponding to the 0.3 M LiFSI, 0.35 M DME in DFM electrolyte. Two replicas were created, and simulations for each replica were started from different levels of aggregation in the electrolytes. Equilibration runs were 20–170 ns followed by 20–140 ns production runs for all simulated systems (Table S3). Multiple timestep integration was employed with timestep of 0.5 fs for bonded interactions, time step of 1.5 fs for all non-bonded interactions within a truncation distance of 8.0 Å and an outer timestep of 3.0 fs for all non-bonded interactions between 8.0 Å and the nonbonded truncation distance of 18 Å. The Ewald summation method was used for the electrostatic interactions between permanent charges with permanent charges or induced dipole moments with $k = 7^3$ vectors. The reciprocal part of Ewald was calculated every 3.0 fs. Induced dipoles were found self-consistently with convergence criteria of 10^{-9} (electron charge * Å) [2].

The MD source code and input files are attached in a separate zip file. Documentation describing all MD simulation files is available at: https://pubs.acs.org/doi/suppl/10.1021/acs.jpcc.8b05573/suppl_file/jp8b05573_si_004.pdf.

CRediT authorship contribution statement

Daniel M. Davies: conceived the idea and designed the experiments, designed and conducted the spectroscopic experiments, conducted the electrochemical experiments, wrote the manuscript with significant contributions of O.B., Y. Yang and other co-authors. **Yangyuchen Yang:** conceived the idea and designed the experiments, designed and constructed the electrolyte addition and housing processes for the 18650 cell, conducted the electrochemical experiments. **Ekaterina S. Sablina:** conducted the electrochemical experiments. **Yijie Yin:** conducted the electrochemical experiments. **Matthew Mayer:** conducted the electrochemical experiments. **Yihui Zhang:** conducted the electrochemical experiments. **Jungwoo Z. Lee:** led the nail penetration testing. **Bingyu Lu:** conducted the electrochemical experiments. **Dijo Damien:** carried out the MD simulations with the help of M.O. **Oleg Borodin:** developed force field and O.B. and D.M.D. carried out the MD simulations with the help of M.O. **Cyrus S. Rustomji:** conceived the idea and designed the experiments, designed and constructed the electrolyte addition and housing processes for the 18650 cell, led the nail penetration testing. **Y. Shirley Meng:** conceived the idea and designed the experiments, wrote the manuscript with significant contributions of O.B., Y. Yang and other co-authors.

Declaration of competing interest

The authors declare the following financial interests/personal relationships which may be considered as potential competing interests: Patent applications relating to this work include PCT/US14/066015, PCT/US17/29821, PCT/US2019/032414, and PCT/US2019/032413. Y. Shirley Meng is a member of the scientific advisory board for South 8 Technologies.

Acknowledgements

This work was supported by South 8 Technologies under National Science Foundation NSF SBIR program (grant no. 1721646). Partial funding for the advanced characterization is provided by the Assistant Secretary for Energy Efficiency and Renewable Energy, Office of Vehicle Technologies of the U.S. Department of Energy under the Battery500 Consortium. The authors gratefully acknowledge R. Chen for use of facilities for much of the scope of this work. The authors acknowledge the use of facilities and instrumentations supported by NSF through the UC San Diego Materials Research Science and Engineering Center(UCSD MRSEC), DMR-2011924. Work at ARL by O. Borodin was supported as part of the Joint Center for Energy Storage Research, an Energy Innovation Hub funded by the U.S. Department of Energy, Office of Science, Basic Energy Sciences through IAA SN2020957. The authors would like to thank Energy Assurance for the nail penetration testing. The authors would also like to thank Emma S. Zorensky and David F. Zorensky for their help in editing the paper. All experimental and computational data described in the paper are presented, curated, and archived in Cloud Storage system. Raw data and metadata are available upon request.

Appendix A. Supplementary data

Supplementary data to this article can be found online at https://doi.org/10.1016/j.jpowsour.2021.229668.

References

[1] J.B. Goodenough, Y. Kim, Challenges for rechargeable Li batteries, Chem. Mater. 22 (2010) 587–603.
[2] K. Mizushima, P.C. Jones, P.J. Wiseman, J.B. Goodenough, Lixcoo2 (O less-than X less-than-or-equal-to 1) - a new cathode material for batteries of high-energy density, Solid State Ionics 3–4 (1981) 171–174.
[3] M.S. Whittingham, Lithium batteries and cathode materials, Chem. Rev. 104 (2004) 4271–4302.
[4] K. Turcheniuk, D. Bondarev, V. Singhal, G. Yushin, Ten years left to redesign lithium-ion batteries, Nature 559 (2018) 467–470.
[5] B. Liu, J.G. Zhang, W. Xu, Advancing lithium metal batteries, Joule 2 (2018).
[6] X.-B. Cheng, R. Zhang, C.-Z. Zhao, Q. Zhang, Toward safe lithium metal anode in rechargeable batteries: a review, Chem. Rev. 117 (2017) 10403–10473.
[7] W. Xu, et al., Lithium metal anodes for rechargeable batteries, Energy Environ. Sci. 7 (2014) 513–537.
[8] K. Xu, Nonaqueous Liquid Electrolytes for Lithium-Based Rechargeable Batteries, 2004, https://doi.org/10.1021/cr030203g.
[9] F. Ding, et al., Effects of carbonate solvents and lithium salts on morphology and coulombic efficiency of lithium electrode, J. Electrochem. Soc. 160 (2013), https://doi.org/10.1149/2.100310jes.
[10] D. Aurbach, et al., Review on electrode-electrolyte solution interactions, related to cathode materials for Li-ion batteries, J. Power Sources 165 (2007) 491–499.
[11] J. Liu, et al., Pathways for practical high-energy long-cycling lithium metal batteries, Nat. Energy 4 (2019) 180–186.
[12] A. Mauger, M. Armand, C.M. Julien, K. Zaghib, Challenges and issues facing lithium metal for solid-state rechargeable batteries, J. Power Sources 353 (2017) 333–342.
[13] C.S. Rustomji, et al., Liquefied gas electrolytes for electrochemical energy storage devices, Science 356 (2017), eaal4263.
[14] Yangyuchen Yang, M. Daniel, Davies, Yijie Yin, Oleg Borodin, Jungwoo Lee, Chengcheng Fang, Marco Olguin, Xuefeng Wang, Yihui Zhang, Katya Sablina, Cyrus, Rustomji, Y.S. M, High efficiency lithium metal anode enabled by liquefied gas electrolytes, Joule 3 (8) (2019) 1986–2000.
[15] Y. Yang, et al., Liquefied gas electrolytes for wide-temperature lithium metal batteries, Energy Environ. Sci. (2020), https://doi.org/10.1039/D0EE01446J.
[16] L. Suo, et al., Fluorine-donating electrolytes enable highly reversible 5-V-class Li metal batteries, Proc. Natl. Acad. Sci. U. S. A 115 (2018) 1156–1161.
[17] E.C. Castillo, Standards for electric vehicle batteries and associated testing procedures, Adv. Batter. Technol. Electr. Veh. (2015) 469–494, https://doi.org/10.1016/B978-1-78242-377-5.00018-2.
[18] R. Zhao, J. Liu, J. Gu, A comprehensive study on Li-ion battery nail penetrations and the possible solutions, Energy 123 (2017) 392–401.
[19] B. Mao, H. Chen, Z. Cui, T. Wu, Q. Wang, Failure mechanism of the lithium ion battery during nail penetration, Int. J. Heat Mass Tran. 122 (2018) 1103–1115.
[20] Electrochemical Cell Cap, 2019.
[21] C.S. Rustomji, et al., Liquefied gas electrolytes for electrochemical energy storage devices, Science 80– (2017) 356.
[22] NIST WebBook. https://webbook.nist.gov/.
[23] ASHRAE, Designation and Safety Classification of Refrigerants, 2018. https://www.ashrae.org/File Library/Technical Resources/Standards and Guidelines/Standards Addenda/34_2016_g_20180628.pdf.
[24] ISO - ISO 817:2014 - Refrigerants — Designation and safety classification. https://www.iso.org/standard/52433.html.
[25] K. Takizawa, A. Takahashi, K. Tokuhashi, S. Kondo, A. Sekiya, Burning velocity measurement of HFC-41, HFC-152, and HFC-161 by the spherical-vessel method, J. Fluor. Chem. 127 (2006) 1547–1553.
[26] Airgas. *Safety*, Data sheet methyl fluoride. https://www.airgas.com/msds/001154.pdf.
[27] P.A. Domanski, M.O. McLinden, I.H. Bell, G.T. Linteris, Low-GWP Alternative Refrigerant Blends for HFC-134a, 2018, https://doi.org/10.6028/NIST.TN.2014. https://nvlpubs.nist.gov/nistpubs/TechnicalNotes/NIST.TN.2014.pdf.
[28] L. Hu, et al., Considerable contribution of the Montreal Protocol to declining greenhouse gas emissions from the United States, Geophys. Res. Lett. 44 (2017) 8075–8083.
[29] AHRI Air-Conditioning, Heating, & Refrigeration Institute. Risk Assessment of Refrigeration Systems Using A2L Flammable Refrigerants. http://www.ahrinet.

org/App_Content/ahri/files/RESEARCH/Technical Results/AHRI-8009_Final _Report.pdf.
[30] J. Calm, G.C. Hourahan, Physical, safety, and environmental data for current and alternative refrigerants, Refrig. Sustain. Dev. (2011).
[31] Wilson, D. P. & Richard, R. G. Determination of refrigerant lower flammability limits in compliance with proposed addendum p to standard 34. ASHRAE Trans. **108,** 739–755.
[32] EPA. Transitioning to Low-GWP Alternatives in Commercial Refrigeration. https://www.epa.gov/sites/production/files/2016-12/documents/international_transitioning_to_low-gwp_alternatives_in_commercial_refrigeration.pdf.
[33] S. Hess, M. Wohlfahrt-Mehrens, M. Wachtler, Flammability of Li-ion battery electrolytes: flash point and self-extinguishing time measurements, J. Electrochem. Soc. 162 (2015) A3084–A3097.
[34] Safety Data Sheet. https://www.iofina.com/static/chemical_files/Methyl_Fluoride-Iofina_Chemical_SDS_11-7-13.pdf.
[35] T.T. Hagos, et al., Locally concentrated LiPF6 in carbonate-based electrolyte with fluoroethylene carbonate as a diluent for anode-free lithium metal battery, ACS Appl. Mater. Interfaces acsami (2019) 8b21052, https://doi.org/10.1021/acsami.8b21052.
[36] X. Ren, et al., High-concentration ether electrolytes for stable high-voltage lithium metal batteries, ACS Energy Lett (2019) 896–902, https://doi.org/10.1021/acsenergylett.9b00381.
[37] * Nikolay Goutev, Keiichi Ohno, H. Matsuura, Raman Spectroscopic Study on the Conformation of 1,2-Dimethoxyethane in the Liquid Phase and in Aqueous Solutions, 2000, https://doi.org/10.1021/JP001340+.
[38] D. Brouillette, et al., Stable solvates in solution of lithium bis (trifluoromethylsulfone)imide in glymes and other aprotic solvents: phase diagrams, crystallography and Raman spectroscopy Electronic supplementary information (ESI) available: crystallographic data (single crystal data) in cif format (CCDC reference number 184345), Phys. Chem. Chem. Phys. 4 (2002) 6063–6071. http://www.rsc.org/suppdata/cp/b2/b203776a/.
[39] S.-D. Han, O. Borodin, D.M. Seo, Z.-B. Zhou, W.A. Henderson, Electrolyte solvation and ionic association, J. Electrochem. Soc. 161 (2014) A2042–A2053.
[40] Y. Yamada, M. Yaegashi, T. Abe, A. Yamada, A superconcentrated ether electrolyte for fast-charging Li-ion batteries, Chem. Commun. 49 (2013) 11194.
[41] S.-D. Han, O. Borodin, D.M. Seo, Z.-B. Zhou, W.A. Henderson, Electrolyte solvation and ionic association, J. Electrochem. Soc. 161 (2014) A2042–A2053.
[42] O. Borodin, Polarizable force field development and molecular dynamics simulations of ionic liquids, J. Phys. Chem. B 113 (2009) 11463–11478.
[43] L. Suo, et al., Water-in-salt" electrolyte enables high-voltage aqueous lithium-ion chemistries, Science 350 (2015) 938–943.
[44] F. Wu, et al., Boosting high-performance in lithium-sulfur batteries via dilute electrolyte, Nano Lett. 20 (2020) 5391–5399.
[45] O. Borodin, et al., Insights into the structure and transport of the lithium, sodium, magnesium, and zinc bis(trifluoromethansulfonyl)imide salts in ionic liquids, J. Phys. Chem. C 122 (2018) 20108–20121.